Bi, Qilong; Shen, Xiaoteng; Lee, Byung Joon; Toorman, Erik

Investigation on estuarine turbidity maximum response to the change of boundary forcing using 3CPBE flocculation model

Investigation on estuarine turbidity maximum response to the change of boundary forcing using 3CPBE flocculation model

Qilong Bi[1,2], Xiaoteng Shen[3], Byung Joon Lee[4] and Erik Toorman[2]

[1] Flanders Hydraulics Research, Antwerp, Belgium.
[2] Hydraulics Section, Department of Civil Engineering, KU Leuven, Leuven, Belgium.
[3] College of Harbour, Coastal and Offshore Engineering, Hohai University, Nanjing, China.
[4] Department of Construction and Environmental Engineering, Kyungpook National University, Sangju, South Korea.

Email: qilong.bi@mow.vlaanderen.be

***Abstract*—Seasonal variation in suspended particular matter (SPM) is often observed in the Scheldt estuary. As part of it, the estuarine turbidity maximum (ETM) zone also exhibits different characteristics in different periods of a year. There are many reasons behind this complex phenomenon, the change of boundary forcing and the biological effects. This study tries to understand the ETM response to the change of boundary forcing in a seasonal scale. For this purpose, a schematic model of the Scheldt estuary is created, and a 3-class population balance equation based (3CPBE) flocculation model is incorporated. The model results reveal that the flocculation process is crucial for reproducing the ETM, and more importantly, its seasonal variation.**

I. INTRODUCTION

The Sea Scheldt is an upper part of the Scheldt Estuary. Unlike the downstream part of the estuary, i.e. the Western Scheldt (0-60 km), the Sea Scheldt (60-160 km) can be considered as a single channel system with tidal influence, stretching from the Dutch/Belgian border to the upstream boundary at Gent (Schepers et al. 2018). Although three main tributaries, i.e. the Dender, the Durme, and the Rupel, join the Sea Scheldt at its upstream (Figure 1), their contributions to the total discharge is usually limited.

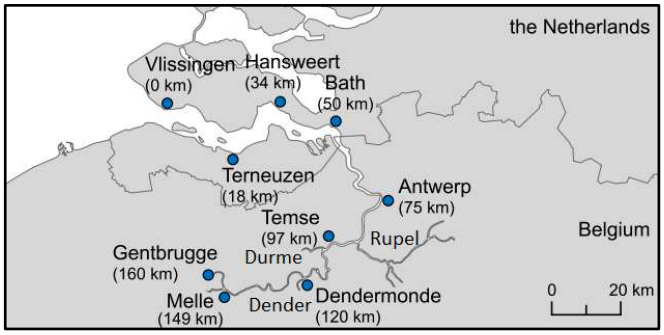

Figure 1 – Overview of the Scheldt estuary (Dijkstra et al., 2017)

Two estuary turbidity maximum (ETM) zones are often observed in the Sea Scheldt, the first one is located near Oosterweel, which is downstream of the city of Antwerp, and the second one about 100 km to 140 km from Vlissingen (Vandenbruwaene et al. 2018). The first ETM is heavily influenced by the human interventions, e.g. dredging/dumping activities, while the second ETM is usually more subjected to the tidal forcing and the upstream discharges. This study only focusses on the second ETM in the Sea Scheldt.

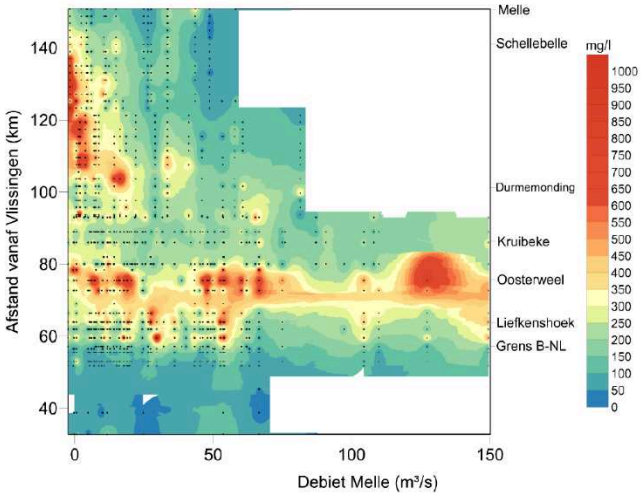

Figure 2 - Near surface sediment concentration at half-tide ebb along the Sea Scheldt in relation to the flow discharge at Melle based on all measurements since the year 2009 (source: Vandenbruwaene et al. 2018).

The long-term observation confirms that the second ETM tends to move landward and extends its length towards the upstream boundary during summer when the daily-averaged discharge is low (< 20 m3/s), whereas it moves towards the downstream with shorter length during winter when the daily-averaged discharge becomes larger (> 35 m^3/s) (Figure 2). This seasonal variation of spatial patterns also comes with other changes in the water column. Some other field measurements show that the sediment density varies between summer and winter conditions. To be more specific, the sediment particles observed at Schellebelle (about 140 km

from Vlissingen) exhibit smaller density and larger size, hence, larger settling velocity during summer. This implies that flocculation may play a role in the seasonal variation in suspended particulate matter (SPM) in the Sea Scheldt, especially in the second ETM.

There could be many reasons for the seasonal variations of the ETM observed in the Sea Scheldt. One of the reasons is the changes of boundary forcing from winter to summer, especially the discharge at the upstream boundary. The boundary forcing could influence the hydrodynamics in several ways, e.g. alter the tidal asymmetry, shift the convergence point between the tide-energy and river-energy, and change the local flow conditions. In reality, as one of the important properties of cohesive sediments, flocculation is inevitably subject to these hydrodynamic changes as well since turbulent shear is one of the main factors controlling aggregation and breakage of flocs. This will further affect the settling velocity and density of these cohesive particles, hence, the transport process and SPM distribution, which could influence the flocculation in a feedback loop. Another possible reason for the seasonal variation of the ETM is the biological activities, which are usually high in summer and low in winter. The biomass in the water system, therefore, is under influence of the biological activities, and could be linked to the aggregation and breakage of flocs through a so-called bio-mediated flocculation (Lee et al. 2017).

Traditional sediment transport models usually have difficulties in capturing the seasonal variation of the ETM in riverine and estuarine systems due to simplified assumptions of sediment properties, e.g. uniform and constant particle size density, and settling velocity. This restricts the models reacting to the changes of boundary forcing and other conditions in a more dynamic and realistic way. Some models employ flocculation models to overcome this issue. However, the flocculation models used are either based on empirical formulas or assumptions under equilibrium conditions, which are still not ideal.

This study employs a dynamic approach for modelling flocculation process. This approach is based on a set of multiple population balance equations (MPBEs), with carefully designed source and sink terms for capturing flocculation kinetics (Lee et al. 2011; Shen et al. 2018). Instead of only tracking the floc size, this approach considers 2 classes (2CPBE) or 3classes (3CPBE) of flocs, and utilizes a set of coupled PBEs for describing the aggregation and breakage of flocs due to Brownian motion, turbulent shear and differential settling. In this case, the number concentration of each floc class is tracked, as well as the composition of the particles. Based on this approach, a schematic model of Scheldt estuary is created and used for investing the seasonal variation of SPM and the ETM response to the boundary forcing. The biological effects are not considered in this study for simplicity.

II. METHODOLOGY

A 3D schematic model for the Scheldt estuary is created in this study using a customized version of the openTELEMAC modelling suite, in which multiple versions of the MCPBE flocculation model (2CPBE model and two variations of 3CPBE models) have been implemented, with additional optimizations for large-scale applications (Bi et al. 2019). The code development allows complex 3D sediment transport modelling, e.g. mixed sediment transport with multiple cohesive and/or non-cohesive classes. Transport of cohesive sediment (with two or three floc size classes) can be modelled as suspended load with flocculation kinetics enabled, while transport of non-cohesive sediment is modelled as bedload.

A 3-class cohesive sediment transport model is coupled with hydrodynamics, in which the interactions between the 3 sediment (floc) classes are accounted through the aggregation and breakage processes modelled by the 3CPBE flocculation model (Shen et al. 2018). Sediment properties, e.g. particle density and settling velocity, can be altered due to various control parameters, such as flow strength, local sediment size distribution and SPM concentration. This would allow the modelled system reacting to the boundary forcing in a more realistic way and provide the possibility of capturing the seasonal variations of SPM often observed in nature.

A. Hydrodynamics

The hydrodynamics in TELEMAC-3D is modelled with the 3D incompressible Reynolds-averaged Navier-Stokes equations. The Navier–Stokes equations for incompressible flows consist of two equations: the continuity equation and the momentum equation. Assuming that the fluid density is constant, and applying the Boussinesq eddy viscosity approximation to the Reynolds stress term, the mass and momentum conservation equations read:

$$\nabla \cdot \mathbf{u} = 0 \tag{1}$$

$$\frac{\partial \mathbf{u}}{\partial t} + (\mathbf{u} \cdot \nabla)\mathbf{u} = -\frac{1}{\rho}\nabla p + \nabla \cdot [(\nu + \nu_T)\nabla \mathbf{u}] + \mathbf{g} + \mathbf{F} \tag{2}$$

where $\mathbf{u}$ is the Reynolds-averaged mean velocity field, t is the time, ρ is the fluid density, p is the mean pressure, ν is the kinematic viscosity of the fluid, ν_T is the turbulence eddy viscosity, $\mathbf{g}$ is the gravitational force and $\mathbf{F}$ represents the other external forces, e.g. Coriolis force and centrifugal force.

Several turbulence models are available in the TELEMAC-3D. The most commonly used ones are the $k-\epsilon$ model, the Smagorinski model and the mixing-length model. It is also possible for the users to define constant eddy viscosity for horizontal and vertical, respectively. In this study the *k*-ϵ model is adopted in all the simulations.

B. Sediment transport with flocculation

This study adopts the 3CPBE flocculation model (Shen et al. 2018), which is an improvement to the 2CPBE flocculation model (Lee et al. 2011) and applies it to a 3D application. Similar to the 2CPBE flocculation model, by including one more sediment class, the 3CPBE flocculation model is able to describe the flocculation dynamics with the representative sizes and mass fractions of microflocs (≤ 30 μm), macroflocs ($30 - 300$ μm) and megaflocs (≥ 300 μm).

In the 3CPBE flocculation model, the microflocs belongs to the smallest class among the three. Because of its compact structure, microflocs are relatively stable in the environment and difficult to be further broken-up. Thus, it acts as the basic

building block for the other two sediment classes. Usually a fixed particle size derived from the field measurements is assigned to the microflocs, therefore, its particle density also remains constant.

The megaflocs are categorized as the largest class among the three and usually have variable sizes and densities depending on their compositions. For simplicity, in this study the megaflocs are also considered as a fixed-sized class. A representative particle size based on the field measurements is assigned to this class.

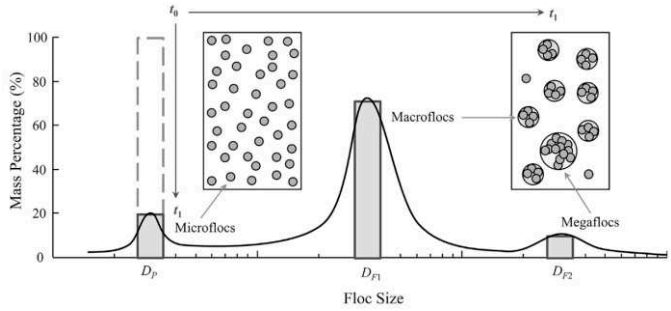

Figure 3 - Schematic diagram of the FSDs before and after flocculation (Shen et al. 2018). At time t_0, all particles are concentrated on microflocs. With time, macroflocs and megaflocs have appeared because of aggregation and breakage processes.

The governing equations of the 3CPBE flocculation model in 3D are described as follows:

$$\frac{\partial N_i}{\partial t} + (\mathbf{u}\cdot\nabla)N_i = \nabla\cdot\left(D_T\nabla N_i + \mathbf{w_{s,i}}N_i\right) + (A_i + B_i) \qquad (3)$$

where N_i is the number concentration of class *i (i=P, F1, T1 or T2)*, $\mathbf{u}$ is the Reynolds-averaged mean velocity vector, t is the time, D_T is the turbulent diffusion coefficient, $\mathbf{w_{s,i}}$ is the settling velocity vector of class *i* pointing downward, A_i and B_i are aggregation and breakage source and sink terms. Eq.(3) is a system of coupled transport equations that track (1) the number of microflocs and macroflocs in suspension per unit volume, with symbol N_P and N_{F1} respectively, (2) the total number of microflocs in all macroflocs per unit volume N_{T1}, and (3) the total number of microflocs in all megaflocs per unit volume N_{T2}.

It is worth mentioning that the eq.(3) is slightly modified when implemented in the openTELEMAC. The main reason is that the number concentration N_i is usually much larger than the other variables and could cause instability when solved in a coupled way with other unknown variables in TELEMAC-3D. The solution is to rescale N_i by multiplication both side of with the mass of one microfloc m_p (a constant value), thus, eq.(3) can be written as:

$$\frac{\partial C_P}{\partial t} + (\mathbf{u}\cdot\nabla)C_P = \nabla\cdot\left(D_T\nabla C_P + \mathbf{w_{s,i}}C_P\right) + m_p(A_P + B_P) \qquad (4)$$

$$\frac{\partial C_{F1}}{\partial t} + (\mathbf{u}\cdot\nabla)C_{F1} = \nabla\cdot\left(D_T\nabla C_{F1} + \mathbf{w_{s,i}}C_{F1}\right) + m_p(A_{F1} + B_{F1}) \qquad (5)$$

$$\frac{\partial C_{T1}}{\partial t} + (\mathbf{u}\cdot\nabla)C_{T1} = \nabla\cdot\left(D_T\nabla C_{T1} + \mathbf{w_{s,i}}C_{T1}\right) + m_p(A_{T1} + B_{T1}) \qquad (6)$$

$$\frac{\partial C_{T2}}{\partial t} + (\mathbf{u}\cdot\nabla)C_{T2} = \nabla\cdot\left(D_T\nabla C_{T2} + \mathbf{w_{s,i}}C_{T2}\right) + m_p(A_{T2} + B_{T2}) \qquad (7)$$

with $C_P = m_p N_P$, $C_{F1} = m_p N_{F1}$, $C_{T1} = m_p N_{T1}$ and $C_{T2} = m_p N_{T2}$. By definition, C_P, C_{T1}, and C_{T2} are equivalent to the mass concentration of microflocs, macroflocs, and megaflocs, respectively, while C_{F1} does not have a specific physical meaning. Note that eqs.(4) – (7) not only describe the flocculation process, i.e. aggregation and breakage of flocs, but also the transport of microflocs, macroflocs and megaflocs.

TABLE 1 - AGGREGATION AND BREAKAGE PROCESSES OF SUSPENDED PARTICLES WITH THREE SIZE GROUPS (SHEN ET AL. 2018).

Processes (j) ↓	Description
(1) Aggregation *Microflocs & Microflocs*	
(2) Aggregation *Microflocs & Macroflocs*	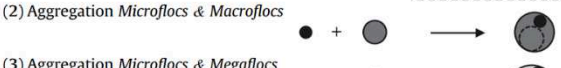
(3) Aggregation *Microflocs & Megaflocs*	
(4) Aggregation *Macroflocs & Macroflocs*	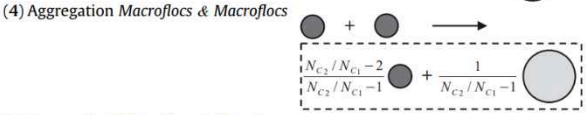
(5) Aggregation *Macroflocs & Megaflocs*	
(6) Breakage *Macroflocs*	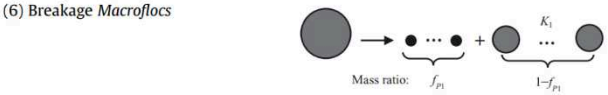
(7) Breakage *Megaflocs*	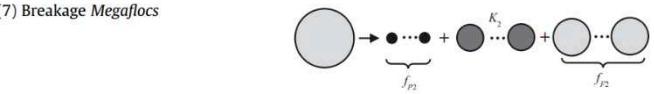

The flocculation processes included in this 3CPBE flocculation model are summarized in Table 1, with five aggregation processes and two breakage processes (Shen et al. 2018). The flocculation processes are modelled in the source and sink terms as follows.

$$(A_p + B_p) = -\frac{1}{2}\alpha\beta_{PP}N_P N_P\left(\frac{N_{C1}}{N_{C1}-1}\right) - \alpha\beta_{PF1}N_P N_{F1} - \alpha\beta_{PF2}N_P N_{F2} + f_{P1}N_{C1}a_{F1}N_{F1} + f_{P2}N_{C2}a_{F2}N_{F2} \qquad (8)$$

$$(A_{F1} + B_{F1}) = \frac{1}{2}\alpha\beta_{PP}N_P N_P\left(\frac{1}{N_{C1}-1}\right) - \frac{1}{2}\alpha\beta_{F1F1}N_{F1}N_{F1}\left(\frac{N_{C2}/N_{C1}}{N_{C2}/N_{C1}-1}\right) - \alpha\beta_{F1F2}N_{F1}N_{F2} + (K_1-1)a_{F1}N_{F1} + K_2 a_{F2}N_{F2} \qquad (9)$$

$$(A_{T1} + B_{T1}) = \frac{1}{2}\alpha\beta_{PP}N_P N_P\left(\frac{N_{C1}}{N_{C1}-1}\right) + \alpha\beta_{PF1}N_P N_{F1} - \frac{1}{2}\alpha\beta_{F1F1}N_{F1}N_{F1}\left(\frac{N_{C2}/N_{C1}}{N_{C2}/N_{C1}-1}\right) - N_{C1}\alpha\beta_{F1F2}N_{F1}N_{F2} - f_{P1}N_{C1}a_{F1}N_{F1} + (1-f_{P2}-f_{F2})f_{P2}N_{C2}a_{F2}N_{F2} \qquad (10)$$

$$(A_{T2} + B_{T2}) = \alpha\beta_{PF2}N_P N_{F2} + \frac{1}{2}\alpha\beta_{F1F1}N_{F1}N_{F1}\left(\frac{N_{C2}/N_{C1}}{N_{C2}/N_{C1}-1}\right) + N_{C1}\alpha\beta_{F1F2}N_{F1}N_{F2} - (1-f_{P2})N_{C2}a_{F2}N_{F2} \qquad (11)$$

where *P, F1, F2, T1* and *T2* are the indices for microflocs, macroflocs, megaflocs, microflocs in macroflocs and microflocs in megaflocs, N_i is the number concentration (*i=P, F1, F2, T1* or *T2*), α is the collision efficiency, β_{ij} is the collision frequency (*i,j=P, F1, F2, T1* or *T2*), a_i is the breakup frequency concentration (*i= F1 or F2*), $N_{C1}=N_{T1}/N_{F1}$ the number of micflocs bonded in a macrofloc, $N_{C2}=N_{T2}/N_{F2}$ the number of micflocs bonded in a megafloc (for fixed size of megaflocs, N_{C2} is a constant), f_{P1} is the mass fraction of created microflocs when a macrofloc breaks up, f_{P2} is the mass fraction of created microflocs when a megafloc breaks up, f_{F2} is the mass fraction of the remaining megafloc when a larger megafloc breaks up, K_1 is the number of created macroflocs when a larger macrofloc breaks up, K_2 is the number of generated macroflocs when a megafloc breaks up.

The collision efficiency α is a fitting parameter, and the collision frequency β_{ij} can be expressed as (Thomas et al., 1999; Maggi, 2005) with a linear combination of three mechanisms (terms):

$$\beta_{ij} = \frac{1}{6}G\left(D_i + D_j\right)^3 + \frac{\pi}{4}\left(D_i + D_j\right)^2\left|w_{s,i} - w_{s,j}\right| + \frac{2}{3}\frac{K_B T}{\mu}\frac{\left(D_i + D_j\right)^2}{D_i D_j} \quad (12)$$

where G is the shear rate, us is the settling velocity, K_B is the Boltzmann constant, T is the absolute temperature and μ is the fluid dynamic viscosity, D is the particle diameter, w_s is the settling velocity given by a fractal-corrected Stokes equation with hindered settling corrections (Winterwerp and van Kesteren, 2004), i and j are the indices *P, F1, F2, T1* or *T2*. Given the fixed size of microflocs, the sizes of macroflocs and megaflocs can be determined as (Matsoukas and Friedlander, 1991):

$$D_{Fi} = D_P N_{Ci}^{1/nf_i}, \quad i = 1,2 \quad (13)$$

where *nf* is the fractal dimension of flocs, and D_P, D_{F1} and D_{F2} are the characteristic sizes of microflocs, macroflocs and megaflocs, respectively. In the 3CPBE flocculation model used in this study, D_{F2} is also assumed as a constant to reduce the number of tracers. This assumption can be supported by field data used in Shen et al. (2018).

It is important to note that the effect of turbulent shear (the first term in eq.(12)) is the main mechanism in natural environments (Winterwerp, 1998). The effect of differential settling (second term in eq.(12)) is important during slack tide when turbulence is low (Lick et al., 1993), while the effect of Brownian motion (the third term in eq.(12)) is generally low for large particles (Winterwerp, 1998).

The breakup frequency a can be written as (Winterwerp, 1998):

$$a_i = E_b G\left(\frac{D_i - D_P}{D_P}\right)^{3-nf}\left(\frac{\mu G}{F_y/D_i^2}\right)^{1/2} \quad (14)$$

where E_b is the breakage coefficient. The floc strength F_y, although not a constant (Kranenburg, 1999), is assumed 10^{-10} Pa in this study (Maggi et al., 2007; Verney et al., 2011).

The erosion and deposition fluxes have to be computed at the interface between bed layer and water column in order to provide the necessary bottom boundary conditions for the governing equations of 3CPBE flocculation model (eq.(4) – (7)). This is done in GAIA, which is a sediment transport module in the openTelemac suite. Therefore, in order to have a complete 3D sediment transport model, TELEMAC-3D has to be coupled with GAIA.

The following equation is used as the boundary condition near the bed for the suspended sediment transport equation (taken at a reference height z_b above the bed):

$$-D_v\frac{\partial C_i}{\partial z} - w_{s,i}C_i = (E_i - D_i)_{z_b} \quad (15)$$

where D_v is the vertical eddy diffusivity, C_i is the sediment mass concentration of class *i (i=P, F1, T1 or T2)*, z is the vertical coordinate, w_s is the settling velocity, E_i is the erosion flux of class *i* and the deposition flux of class *i* $D_i = w_{s,i}C_i$.

In the 3CPBE flocculation model, it is assumed that macroflocs and megaflocs are destroyed by large shear near the bottom and broken down into microflocs when deposited to the bed. In this case, the bed material only consists of microflocs, which will be the only floc class that can be eroded. Hence, the bottom boundary conditions for eq.(4) – (7) become:

$$-D_v\frac{\partial C_i}{\partial z}\Big|_{z_b} = \begin{cases} E_i & if\ i = P \\ 0 & if\ i = F1, T1\ or\ T2 \end{cases} \quad (16)$$

This is a Neumann type boundary and it states that the diffusive flux is balanced by the erosion flux at the bottom. In TELEMAC-3D, the erosion flux of microflocs is given by:

$$E_p = \max\left(0,\ M\left(\frac{\tau_b}{\tau_c} - 1\right)\right) \quad (17)$$

where, M is the erosion parameter, τ_b is the bed shear stress and τ_c is the critical shear stress for erosion.

III. SCHEMATIZED SCHELDT MODEL

For better understanding the seasonal variation of SPM and the ETM response to the boundary forcing in the Sea Scheldt, and finding out the influence of flocculation processes on the ETM dynamics, a 3D schematized model with six vertical layers based on the measured estuary width and bottom elevation was created.

The 3CPBE flocculation model proposed by Shen et al. 2018 is adopted in this study for modelling the flocculation kinetics. There are two variations of the 3CPBE model, a simplified version assuming a fixed-sized megaflocs, and a more complex version that allows the properties of megaflocs evolving dynamically. The former is applied in the current model for simplicity, while the latter is more suitable for incorporating biological effects, which could also be important processes for the seasonal variation of SPM observed in rivers and coasts (Lee et al. 2017; Fettweis et al. 2017).

In this study, the geometry of the Scheldt Estuary has been schematized by a funnel-shaped domain as in Dijkstra et al.

(2017) and Brouwer et al. (2018), based on observations. As shown in Figure 4, the schematized geometry is derived by fitting an exponential function of a ratio of two polynomials against observed width along the Scheldt estuary. Similarly, the bottom in the schematized domain is obtained by fitting a smooth function to the measured cross-sectionally averaged depth along the estuary. To better approximate the tidal propagation in the estuary, the tidal prism is kept as close as possible to the real estuary. The estuary width is used for deriving the schematised geometry, the bottom is kept flat in cross-channel direction but with longitudinal slope. This synthetic bathymetry is then derived using the measured wet-sections along the estuary, so that the tidal prism will not be altered.

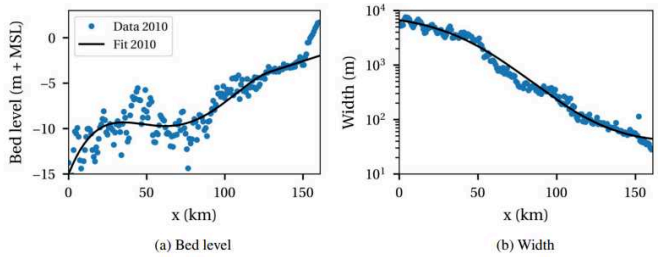

Figure 4 - The measured and fitted geometry of the Scheldt Estuary (Dijkstra et al., 2017)

The schematized domain starts at Vlissingen the estuary mouth and ends all the way up to the Gentbrugge where tidal locks were installed. The total length is 160km. The width is about 13.3km at the mouth and about 90m at the upstream boundary. It is worth mentioning that due to the simplified geometry, the tidal flats are not included, which may result in overestimation of tidal amplitude.

In order to have a lightweight triangular mesh that allows the model running efficiently for long period, the grid size is defined as a function of the width along the estuary (Bi et al. 2020). This results in a mesh that is symmetric about the x-axis. There are always four elements distributed along the y-axis at each kilometre, and those elements are aligned with the streamlines from downstream until the very upstream. The final mesh size ranges from about 4000 m in the estuary mouth to about 30 m in the upstream boundary (Figure 5).

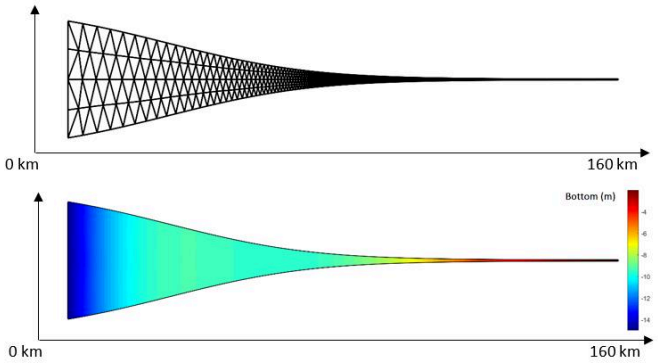

Figure 5 - The Telemac grid and bathymetry of the schematized Scheldt estuary

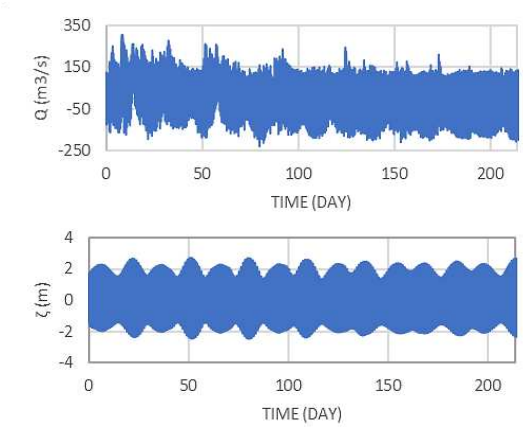

Figure 6 – Boundary conditions of the model (upper: upstream discharge measured at Melle, lower: downstream water level measured at Cadzand)

For the hydrodynamics, the boundary conditions are based on the field measurements in order to provide a better approximation of the tidal forcing. The continuously measured timeseries of water level at Cadzand and freshwater discharge at Melle in 2015 is imposed at downstream (km 0) and upstream (km 160) boundaries, respectively (Figure 6).

For the sediment transport, due to the lack of continuous data at the downstream boundary, the model assumes a so-called equilibrium boundary condition for sediment concentration. Instead of using fixed values, the imposed SPM concentrations at both upstream and downstream boundaries are time-dependent and computed based on the equilibrium condition at the reference level near the bottom, under which the erosion rate is assumed to be the same as the deposition rate. The equilibrium concentration is derived from the 1DV transport equation, in which the eddy diffusivity has a parabolic profile given by the mixing length theory. The concentration profiles imposed at both boundaries are given by Rouse profiles:

$$C(z) = c_b \cdot \left(\frac{z}{H-z}\frac{H-z_b}{z_b}\right)^{-w_s/\kappa u_*} \tag{18}$$

$$c_b = E/w_s \tag{19}$$

in which, ν_t is the eddy viscosity, H is the water depth, z_b is the reference level for the near-bed concentration c_b, w_s is the settling velocity, κ is the von Karman constant and u_* is the shear velocity. The erosion rate E can be computed in a similar way as described in eq.(17). It is worth mentioning that the SPM concentration is only imposed when the water flux pointing inward (coming into the domain), whereas the zero gradient of concentration is imposed when the water flux pointing outward. This type of boundary treatment is called the Thatcher-Harleman boundary condition, which aims to suppress unphysical SPM concentration gradient near open boundaries (Thatcher and Harleman, 1972).

In order to reveal the influence of the flocculation process on the SPM distribution and ETM dynamics, the model is compared with a reference case without flocculation. The other model settings and parameters are listed in Table 2.

TABLE 2 – OVERVIEW OF THE MODEL SET-UPS

Model set-up	Reference case	Model with flocculation
Turbulence model	k-ε model	k-ε model
SPM concentration at boundaries	Eqs.(18) and (19) with z_b=1 cm	The total mass concentration is given by eqs.(18) and (19) with z_b=1 cm, and it is distributed to microflocs (10%), macroflocs (80%) and megaflocs (10%).
Sediment type	cohesive	cohesive
Particle size (µm)	60	Microflocs: 15 Macroflocs: variable Megaflocs: 350
Sediment density (kg/m^3)	1800	Microflocs: 2500 Macroflocs: variable Megaflocs: 1064 (from fractal theory)
Settling velocity (mm/s)	1	Microflocs: 0.18 Macroflocs: variable Megaflocs: 4.1
Critical shear stress for erosion (Pa)	0.4	0.4
Partheniades constant	1.0e-04	1.0e-04

Both the reference model and the model with flocculation start from 01/01/2015 00:00:00 and runs for a period of 7 months covering winter to summer conditions.

IV. RESULTS AND DISCUSSION

The winter and summer conditions in the model is mainly induced by the boundary forcing, which is based on the field measurements. It is known from the data that mean discharge, as shown in Figure 7, is usually much lower in summer (Vandenbruwaene et al. 2018). This change of upstream forcing will further affect tidal asymmetry, flow field, and sediment input from boundaries. If considering the flocculation process, it is no surprise that the floc properties could also react to these changes, exhibiting different characteristics between winter and summer, hence, influencing the SPM distribution under tidal motions.

The model results show that both the reference run and the run with 3CPBE flocculation model could capture the location shift of the second ETM. However, without flocculation, the reference run predicts lower SPM concentration during the entire simulation period, especially in winter condition, and fails to capture the longitudinal growth of the ETM during summer (Figure 2), which is well reproduced in the run with 3CPBE model as seen in Figure 8.

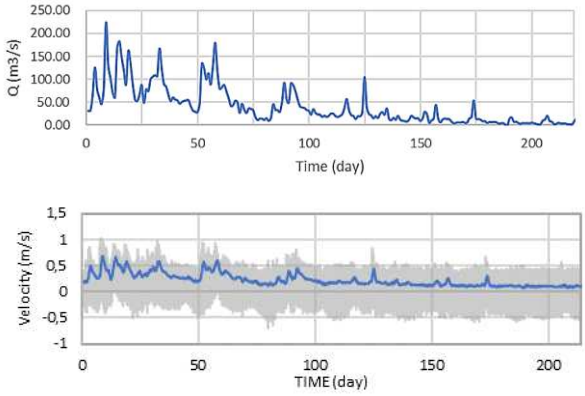

Figure 7 – Daily-averaged upstream discharge measured at Melle in 2015 (upper) and depth-averaged velocity at the upstream boundary with positive values pointing downstream (lower)

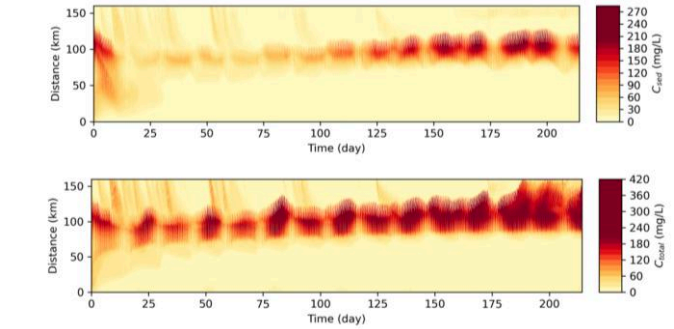

Figure 8 – Evolution of depth-averaged SPM concentration along thalweg of the model from winter to summer
(Upper: reference model, lower: model with flocculation)

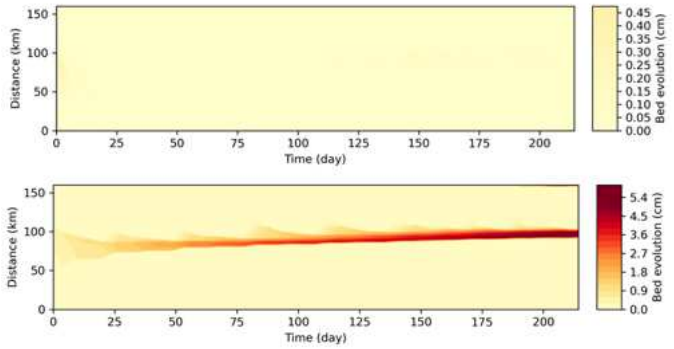

Figure 9 – Bed evolution along thalweg of the model from winter to summer
(Upper: reference model, lower: model with flocculation)

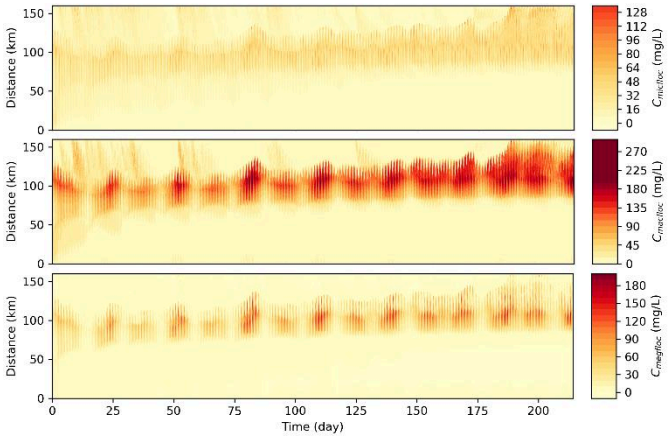

Figure 10 – Evolution of SPM concentration along thalweg from the model with flocculation (Upper:microflocs, middle:macroflocs, lower:megaflocs)

Moreover, higher sedimentation rates are found in the model with flocculation, and the accumulation of bed material occurs in the ETM zone (Figure 9). The bed evolution shows that this bed layer moves towards upstream when ETM zone moves. According to the previous study (Bi et al. 2020), the cumulative bed layer occurs at the location, where the landward net transport rate decreases shapely, it is also where the tidal energy from downstream meets the river energy from upstream (Chen et al. 2005). In the reference model without flocculation, the sedimentation still happens during slack tides, likely forming a weak fluid mud layer, but the deposited sediment is eroded when flow becomes stronger, hence the bed layer is barely accumulated over long period. This suggests that the net sediment transport is altered by the flocculation model, resulting in a higher sediment trapping efficiency in the ETM zone compared to the reference case.

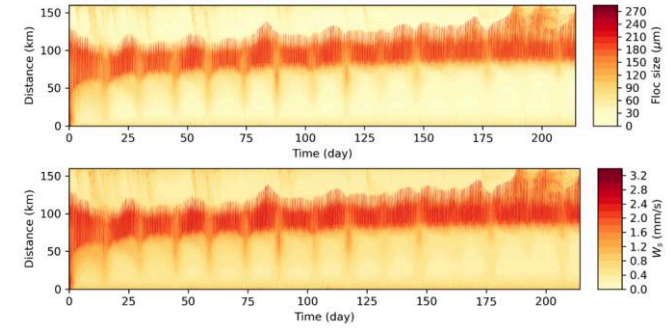

Figure 11 – evolution of mean floc size (upper) and settling velocity (lower) along thalweg of the model with flocculation

One of the advantages of the 3CPBE flocculation model is that it can provide detailed information about how the different sediment groups evolve spatially and temporally in the system and their relations. Figure 10 shows the modelled SPM concentrations of three sediment groups, microflocs, macroflocs and megaflocs, among which the macroflocs are the majority. Further analysis reveals that, with the 3CPBE flocculation model, larger flocs with higher settling velocity can be formed in the ETM zone, whereas outside of this region the smaller flocs with lower settling velocity are found. It also can be seen in Figure 11 that the location of the area with large flocs reacts to the boundary forcing in the same way as the location of ETM zone does, showing the variations during spring-neap cycles as well as in longer period from winter to summer.

The depth-averaged SPM concentrations of three floc size groups along the thalweg of the modelled domain are further analysed by averaging over the winter and summer period, respectively (Figure 12). In winter, the peak SPM concentration is located at 100 km from the estuary mouth. The ETM zone has narrower extent towards upstream and the megaflocs are negligible in the region from 120 km to 160 km. In summer, the peak SPM concentration shifts about 10 km towards upstream and the ETM zone has larger extent towards upstream. The megaflocs also appear in the upstream region, changing the composition of the sediment particles.

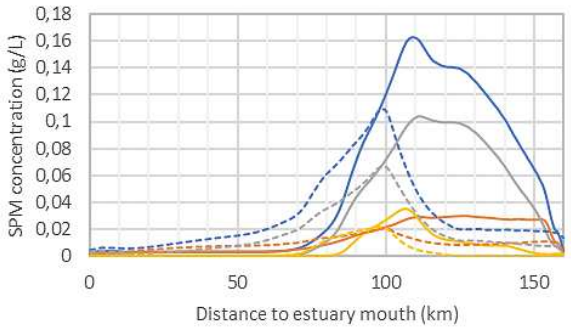

Figure 12 – Depth-averaged SPM concentration along thalweg averaged over winter (dash lines) and summer (solid lines) (blue: total SPM, orange: microflocs, grey: macroflocs, yellow: megaflocs).

In order to understand the seasonal variation of SPM captured by the 3CPBE flocculation model, an upstream boundary node is selected for further examination. The depth-averaged velocity and the SPM concentration is extracted from the model results (Figure 13 and Figure 14).

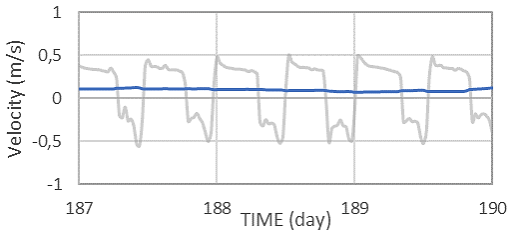

Figure 13 – depth-averaged velocity at upstream boundary in a short period in summer with positive values pointing downstream (grey: instantaneous value, blue: 24H moving average)

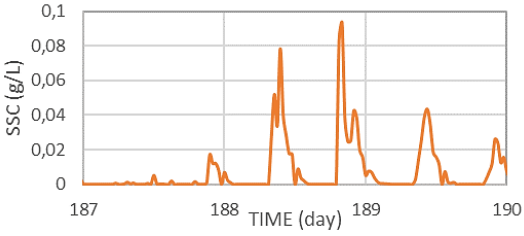

Figure 14 – Depth-averaged total SPM concentrations at the upstream boundary

As seen in the evolution of the depth-averaged velocity at the upstream boundary (Figure 7), the magnitude decreases and the tidal asymmetry changes from winter to summer, with a trend of becoming less ebb dominant. This is one of the reasons that the ETM location shifts towards upstream. In the zoom-in view of a short period in summer (Figure 13 and Figure 14), one can find that the SPM imposed at the upstream boundary only show peaks when the velocity points upstream. Since the Thatcher-Harleman boundary condition is adopted in the model, the SPM concentration can only be caused by advective transport from downstream.

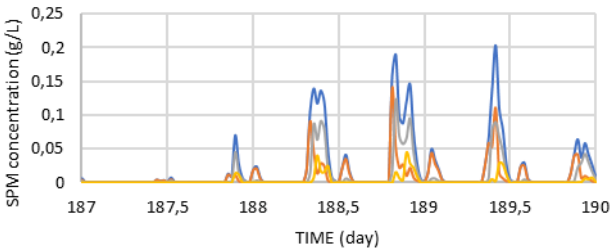

Figure 15 – SPM concentrations of microflocs (orange), macroflocs (grey), megaflocs (yellow) and total SPM concentration (blue) at 159 km

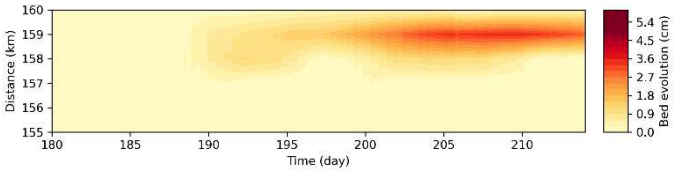

Figure 16 – The zoom-in view of bed evolution near the upstream boundary in a short period in summer

At a location near the upstream boundary (159 km from the estuary mouth), the SPM concentrations of the three floc groups are shown in Figure 15. The change of the boundary forcing results in an environment more favourable for aggregation of flocs. The larger flocs start forming when the sediments being transported from downstream to this location. It is also clear that microflocs appear first during the peak flood velocity, then they form larger flocs during the transition to slack tide and settle down to the bed. This also explains the cause of the sedimentation near the upstream boundary in the same period (Figure 16). It is possible, when the upstream discharge becomes larger, that this cumulated bed layer will be eroded again, providing extra sediment input to the system.

V. CONCLUSION

The analysis of the model results reveals that the flocculation process modelled by the 3CPBE flocculation model is crucial for capturing the seasonal variations of SPM in the upstream region. The modelled system response is close to the field observations.

The results also link the zone with higher settling velocities to the zone with higher SPM concentration in the schematized domain. The comparison with the reference model indicates that only the flocculation model could reproduce reasonable settling velocities in the high concentration area in winter, which are important for maintaining the ETM zone under higher upstream discharge.

From winter to summer, the ETM zone shifts its location towards upstream and increase its extent. This is only reproduced by the model with flocculation. This dynamic behaviour of the ETM is possibly due to several reasons. The change of boundary forcing (lower upstream discharge) leads to a less ebb dominant system, which allows the sediment being transported more landward. The flocculation process enhances this trend by justifying the settling velocity to the local flow conditions and SPM concentrations. The increase of the extent of the ETM zone is only reproduced combing the effect of tidal asymmetry and flocculation process in the model. And this cannot be achieved by using a single value of setting velocity as in the traditional sediment model.

However, it is worth pointing out that due to the lack of tidal flats in the domain, it is unclear how the intertidal area would influence the results. This will be investigated in the future study.

ACKNOWLEDGEMENT

This work is supported by the Flanders Hydraulics Research and Sediment Dynamics group at KU Leuven.

REFERENCES

[1] Bi, Q., Joon Lee, B., Shen, X., Toorman, E., Smolders, S., Vanlede, J. (2019). Implementing MCPBE flocculation models in TELEMAC and investigating the influence of flocculation on large scale sediment transport, in: 15th international conference on cohesive sediment transport processes 13 – 17 October 2019, Istanbul, Turkey (INTERCOH 2019): abstract book. pp. 116-118.

[2] Bi, Q.; Kaptein, S. J.; Schramkowski, G.; Smolders, S.; Mostaert, F. (2020). The iFlow inspired TELEMAC-3D model: Sub report 1 – Comparing ETM dynamics with the iFlow model. Version 2.0. FHR Reports, 19_025_1. Flanders Hydraulics Research: Antwerp.

[3] Brouwer, R. L., Schramkowski, G. P., Dijkstra, Y. M., & Schuttelaars, H. M. (2018). Time evolution of estuarine turbidity maxima in well-mixed, tidally dominated estuaries: The role of availability-and erosion-limited conditions. Journal of Physical Oceanography, 48(8), 1629-1650.

[4] Chen, M. S., Wartel, S., Van Eck, B., & Van Maldegem, D. (2005). Suspended matter in the Scheldt estuary. Hydrobiologia, 540(1-3), 79-104.

[5] Dijkstra, Y. M., Brouwer, R. L., Schuttelaars, H. M., & Schramkowski, G. P. (2017). The iFlow modelling framework v2. 4: a modular idealized process-based model for flow and transport in estuaries. Geoscientific Model Development, 10(7).

[6] Fettweis, M., & Lee, B. J. (2017). Spatial and seasonal variation of biomineral suspended particulate matter properties in high-turbid nearshore and low-turbid offshore zones. Water, 9(9), 694.

[7] Kranenburg, C. (1999). Effects of floc strength on viscosity and deposition of cohesive sediment suspensions. Continental Shelf Research, 19(13), 1665-1680.

[8] Lee, B. J., Toorman, E., Molz, F. J., & Wang, J. (2011). A two-class population balance equation yielding bimodal flocculation of marine or estuarine sediments. Water research, 45(5), 2131-2145.

[9] Lee, B. J., Hur, J., & Toorman, E. A. (2017). Seasonal variation in flocculation potential of river water: Roles of the organic matter pool. Water, 9(5), 335.

[10] Lick, W., Huang, H., Jepsen, R., 1993. Flocculation of fine-grained sediments due to differential settling. J. Geophys. Res.: Oceans 98, 10279-10288.

[11] Maggi, F., 2005. Flocculation Dynamics of Cohesive Sediment (Ph.D. Dissertation). Delft University of Technology, Netherlands.

[12] Maggi, F., Mietta, F., Winterwerp, J.C., 2007. Effect of variable fractal dimension on the floc size distribution of suspended cohesive sediment. J. Hydrol. 343, 43-55.

[13] Matsoukas, T., Friedlander, S.K., 1991. Dynamics of aerosol agglomerate formation. J. Colloid Interface Sci. 146, 495-506.

[14] Schepers, L., Maris, T., Meire, P., & Temmerman, S. (2018). The Scheldt estuary: an overview of the morphodynamics of intertidal areas. In Landscapes and Landforms of Belgium and Luxembourg (pp. 281-296). Springer, Cham.

[15] Shen, X., Lee, B. J., Fettweis, M., & Toorman, E. A. (2018). A tri-modal flocculation model coupled with TELEMAC for estuarine muds both in the laboratory and in the field. Water research, 145, 473-486.

[16] Thatcher, M. L., and D. R. F. Harleman (1972), A mathematical model for the prediction of unsteady salinity intrusion in estuaries, Tech. Rep. 144, Dep. of Civ. Eng., Mass. Inst. of Tecnhol., Cambridge.

[17] Thomas, D.G., Judd, S.J., Frawcett, N., 1999. Flocculation modeling: a review. Water Res. 33, 1579-1592.

[18] Vandenbruwaene, W., Hertoghs, R., Michielsen, S., Van De Moortel, I., Brackx, M., Claeys, S., Plancke, Y., Vereecken, H., Meire, D., Deschamps, M. & Mostaert, F. (2019). Monitoring Effecten Ontwikkelingsschets (MONEOS)–Jaarboek monitoring 2018: factual data rapportage van monitoring waterbeweging en fysische parameters in de Zeeschelde in 2018. WL Rapporten.

[19] Verney, R., Lafite, R., Brun-Cottan, J.C., Le Hir, P., 2011. Behaviour of a floc population during a tidal cycle: laboratory experiments and numerical modelling. Continent. Shelf Res. 31, S64-S83.

[20] Winterwerp, J. C. (1998). A simple model for turbulence induced flocculation of cohesive sediment. Journal of hydraulic research, 36(3), 309-326.

[21] Winterwerp, J. C., & Van Kesteren, W. G. (2004). Introduction to the physics of cohesive sediment dynamics in the marine environment. Elsevier.